AIRBORNE DOPPLER RADAR OBSERVATIONS OF THE MESOSCALE AIR MOTION FIELD IN THE DEVELOPING INNER CORE OF HURRICANE DEBBY

Frank D. Marks, Jr.
Atlantic Oceanographic and Meteorological Laboratory
National Oceanic and Atmospheric Administration
Miami, Florida 33149

Robert A. Houze, Jr.
Department of Atmospheric Sciences
University of Washington
Seattle, Washington 98195

1. INTRODUCTION

At the 21st Conference on Radar Meteorology, we presented a preliminary analysis of the airborne Doppler radar observed wind field in the developing inner core of Hurricane Debby (Marks and Houze, 1983). That study illustrated the potential value of airborne Doppler radar in providing detailed spatial coverage of the wind field in hurricanes. Since the Radar Conference, we have extended and refined the study. The region of the analysis has been extended, additional objective smoothing of the data has been performed, the quality and limitations of the data have been examined, and calculations of vorticity have been added to the analysis. In this paper, we summarize the results obtained through these additional efforts.

2. EXTENDED REGION OF ANALYSIS

Figure 1 shows the flight track (relative to the storm center) of the NOAA WP-3D aircraft for the time period of our analysis (1950-2045 GMT, 14 September 1982) and a composite radar reflectivity pattern derived from the C-band (5 cm wavelength) lower fuselage radar aboard the aircraft. The boxes labelled 1-3 are the regions where dual Doppler radar analyses have been carried out using the measurements from the X-band (3 cm wavelength) Doppler radar located in the tail of the aircraft. The antenna of this radar points normally to the fuselage and sweeps circularly through elevation angles of 0 to 360 deg. When an echo volume is sampled from two different viewing angles, the horizontal wind at that location can be reconstructed, provided that the difference between the two viewing angles is not small and that the flow has not changed significantly in the time between the two observations. The wind fields in Box 1 (constructed from Doppler data collected along the south-north and northeast-southwest flight legs) and Box 2 (constructed from data taken on the northeast-southwest and west-east legs) were described by Marks and Houze (1983). Box 1 covered a portion of the intense developing eyewall, while Box 2 covered a representative portion of the stratiform precipitation located just outside the developing eyewall. In this paper, we have extended the analysis to include Box 3. The winds in this region have been constructed from Doppler data obtained on the west-east and north-south flight legs. This box was ideal since the viewing angles were nearly perpendicular; however, the time elapsed between the two legs was nearly one hour. Thus, only the most stationary features of the field were resolved in Box 3. Inclusion of this box, however, allowed for the analysis of the developing eyewall to be extended southward, where some particularly interesting features of the flow were located.

3. METHODS OF ANALYSIS: INCREASED SMOOTHING OF THE DATA

The methods of locating the X-band radar data in the Cartesian coordinates of each box, unfolding the Doppler velocities, determining the horizontal wind vector at each point, editing the computed velocities and smoothing the calculated wind fields were described by Marks and Houze (1983). These methods remain unchanged in the present paper, except that we have increased the smoothing of the winds. In this study, we have used the two-dimensional Gaussian low-pass Shuman filter given by Eq. (A12) of Ray et al. (1975). This filter has responses of nearly zero, 25 percent and 75 percent at wavelengths of 3, 4 and 8 km, respectively. This smoothing was necessary to remove the effects of transient convective wind fluctuations that may have occurred while the aircraft moved from one viewing position to the next. The times between viewing positions were 8-15 min in Box 1, 19-25 min in Box 2, and 40-50 min in Box 3. Our smoothing seeks to retain only those features which did not change structure significantly over these time periods.

4. DATA QUALITY

We have examined the quality of the data used in this study in two ways: by comparing the Doppler-derived winds at the 0.5 km level with the aircraft winds measured along the flight track at 450 m altitude, and by comparing the Doppler-derived winds in different boxes in regions where the boxes overlapped.

a. Comparison of Doppler-derived Winds at the 0.5 km Level in Different Boxes With Each Other and With Aircraft Winds Measured at the 450 m Level

Doppler-derived winds at 0.5 km are shown with the 450 m level aircraft winds in Fig. 2. The Box 1 Doppler-derived winds are shown in Fig. 2a, with Doppler winds from the

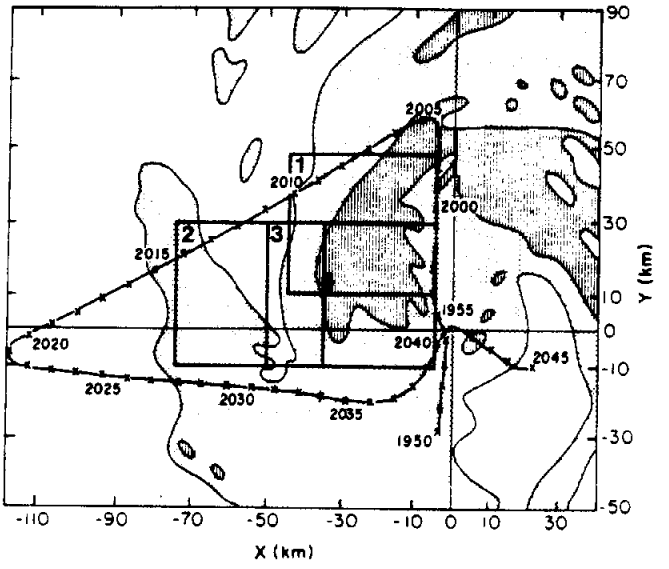

Fig. 1. Temporal composite of the horizontal distribution of reflectivity in Tropical Storm Debby for 1950 - 2045 GMT 14 September 1982. The reflectivity contours are for 20,30 and 40 dBZ. The aircraft flight track is indicated by the thin solid line, and the analysis Boxes 1,2 and 3 are denoted by the thick solid lines. The origin of the coordinate system is located at the storm center, and the aircraft positions have been plotted in relation to the storm center. Coordinates are east-west distance x and north-south distance y from the storm center.

southern part of Box 3 and the aircraft winds along portions of the flight track shown for comparison. The Box 1 winds are highly consistent with the aircraft winds, except in the southeastern corner of Box 1, where the aircraft winds are more easterly than the Box 1 Doppler winds. However, a mesoscale center of cyclonic rotation was located just to the south of this corner of Box 1, and the directional change from easterly along the flight track to northeasterly just inside the corner of the box was at least partly a real spatial variation. The Box 1 winds are also in good agreement with the Box 3 winds. This agreement can be seen along the southern border of Box 1 in Fig. 2a and in Fig. 2b, which shows the complete Box 3 analysis. The entire northern portion of the Box 3 analysis (y = 0 to 30 km) is consistent both with the winds in the corresponding region of Box 1 (Fig. 2a) and with the aircraft winds to the northwest and east.

The winds in the southeastern portion of Box 3 (Fig. 2b) reflect the mesocyclonic circulation and are generally consistent with the aircraft winds, with two exceptions. First, a minor discrepancy is seen in the extreme southeastern corner, where the speeds of the Doppler winds in Box 3 are greater than the speeds of the aircraft winds along the later (south-southwest to north-northeast) flight leg in that vicinity. The speeds of the Box 3 Doppler winds were, however, consistent with the earlier (south to north) flight leg in that region. The second discrepancy is noted where the Doppler winds in the southwestern portion of Box 3 (from x = -25 to -50 km and from y = 0 to -10 km) are in sharp disagreement with the aircraft winds along the west-east flight track south of Box 3. These Doppler winds also strongly disagree with the Doppler winds in the southern part of Box 2 (Fig. 2c). The Doppler winds in the southern part of Box 2 also disagree with the aircraft winds to the south. These Box 2 winds, however, are too easterly, in contrast to those in the southwestern part of Box 3, where the winds are too northerly. Because of the lack of agreement of the southwestern part of Box 3 and the southern part of Box 2 both with each other and with the aircraft winds, little confidence is placed in those regions of analysis.

An additional problem with Box 2 is noted in its northern portion, where the Doppler winds disagree in speed with the aircraft winds along the flight track crossing the northwestern corner of the box.

b. Comparison of Doppler-derived Winds from Different Boxes at Different Altitudes

Doppler-derived winds in the overlap regions of Boxes 1 and 3 and Boxes 2 and 3 have been averaged level-by-level and are compared in Fig. 3. Too few data were present in the overlap region of Boxes 1 and 2 for a similar comparison to be made for these two boxes.

In the Box 1-3 comparison (Fig. 3a), excellent agreement is found at all levels, with Box 3 showing only slightly greater wind speeds. This agreement lends further confidence to the Box 1 winds, which in Sec. 4a were seen also to have agreed well with the aircraft winds.

The Box 2-3 comparison (Fig. 3b) shows sharp disagreement at low levels (below 3 km) and upper levels (above 7 km), with general agreement from 3-7 km. The agreement at middle levels suggests that the poor quality of the winds in the Box 2-3 overlap region noted in Sec. 4a might be mainly a feature of the low and upper-level flow, and that the mid-level winds might be more reliable in these regions. We shall nevertheless in this paper regard the Box 2 winds and the winds in the southwestern portion of Box 3 as suspect and draw conclusions only from the winds in Box 1 and the southeastern portion of Box 3. These regions of

Fig. 2. Doppler-derived winds at 0.5 km level and 450 m level aircraft winds. The latter are plotted along flight tracks labelled at 5 min intervals. Fig. 2(a). Doppler-derived winds in Box 1 (northern box) and Box 3 (only southern part of box is shown). Fig. 2(b). Doppler-derived winds in Box 3.

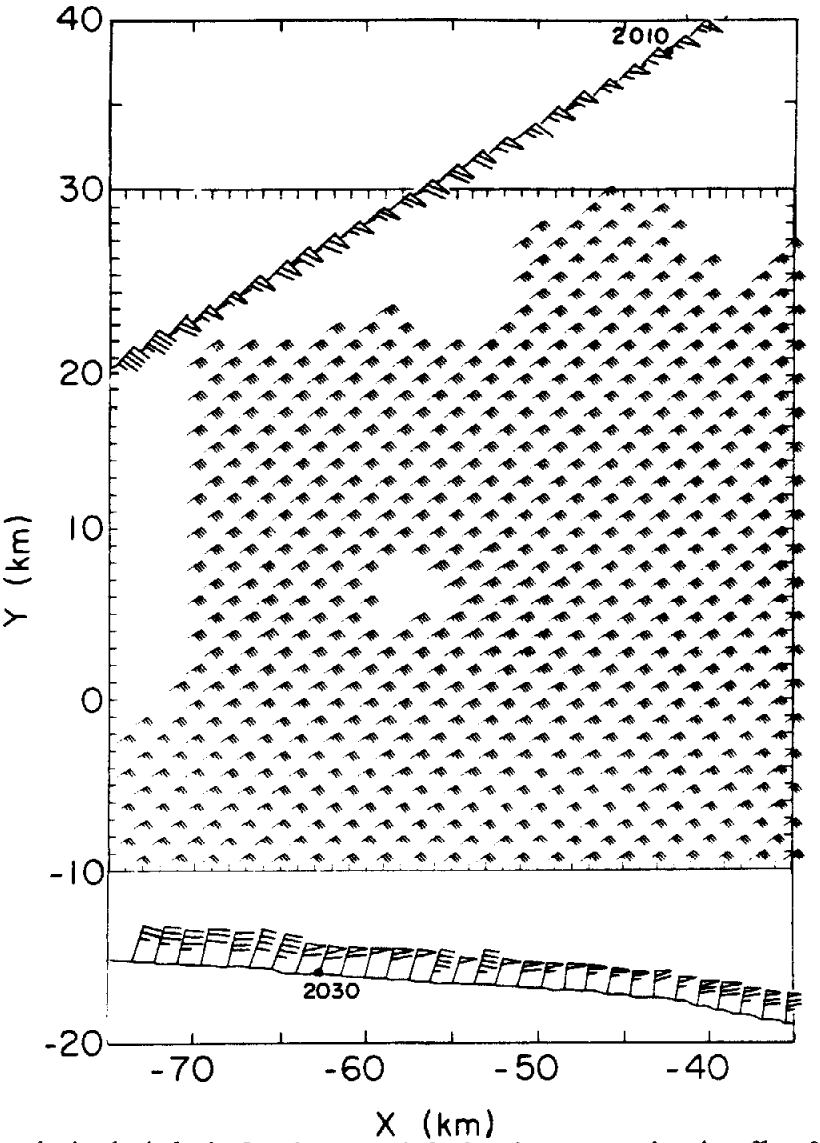

Fig. 2(c). Doppler-derived winds in Box 2. The wind plotting convention is: flag 25 m/s; barb 5 m/s; and half barb 2.5 m/s.

credible winds cover most of the developing eyewall region.

5. ANALYSIS OF THE WIND FIELD AT THE 3 KM LEVEL

To illustrate the results we have obtained, Fig. 4 shows our analysis for the 3 km level. This altitude has been selected for illustration because it was the height at which the mesoscale structure of the wind field associated with the developing eyewall was best defined. Each of the panels of Fig. 4 has been constructed by combining the Box 1 analysis with the southeastern portion of the Box 3 analysis. The analysis shown south of y = 10 km in each panel is from Box 3, while that north of y = 10 km is from Box 1.

In the radar reflectivity field (Fig. 4a), the developing eyewall consisted of a large curved band of intense echo, with several peaks of reflectivity exceeding 40 dBZ. This band extended through the northwestern quadrant of the developing storm. A smaller, more highly curved band lay radially just inward from the larger band. (This smaller band can be seen in the region bounded by x = -10 and -20 km and y = 0 and 20 km in Fig. 4a).

The flow associated with the developing eyewall (Fig. 4b) contained three distinct mesoscale features: two wind speed maxima centered at x = -19 km, y = 37 km, and x = -21 km, y = 17 km, and a mesocyclone centered at x = -20 km, y = 7 km.

Comparison of Figs. 4a and b shows that the two wind maxima lay radially just inward of the axis of maximum radar reflectivity in the large outer rainband. Jorgensen's (1984a,b) recent work with aircraft flight-track data indicates that maximum winds at lower levels tend to occur just inside the reflectivity maximum associated with the eyewall of a mature hurricane. The airborne Doppler winds in Fig. 4b indicate that the maximum winds were already lying just inside the eyewall during its developing phase. The presence of the two separate wind maxima indicates further that the maximum winds were concentrated in

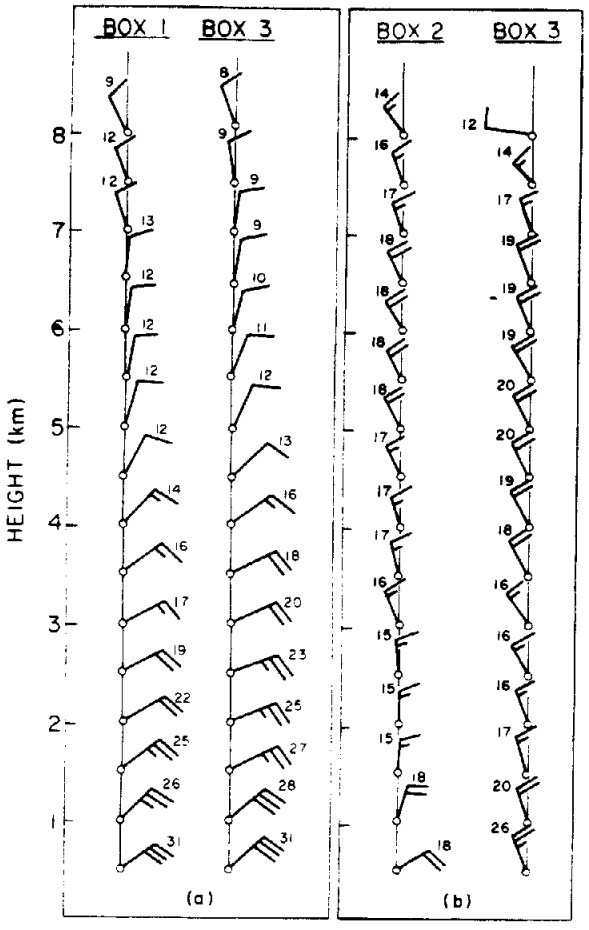

Fig. 3 Mean winds in overlap regions of Boxes 1 and 3 (a) and Boxes 2 and 3 (b) at various altitudes.

discrete mesoscale disturbances along the echo band, and not in a two-dimensional line parallel to the band.

The presence of the mesocyclone indicates that flow around a developing hurricane can be very highly disturbed on the mesoscale. Its structure is suggestive of a breakdown of the storm-scale vortex into sub-vortices revolving around the storm center (analogous to the breakdown of a tornado vortex into suction vortices). The inner sub-band of precipitation seen in Fig. 4a was related to the mesocyclone. The strongest part of the precipitation sub-band extended east-southeastward from the mesocyclone center along the line of confluence extending downwind of the mesocyclone.

The mesocyclone had good vertical continuity. At the 1 km level (not shown), it had a pronounced center, collocated with a weak-echo "eye" at the eastern end of the precipitation sub-band (at x = -9 km, y = 1 km). The mesocyclone center sloped west-northwestward with height, along the axis of the sub-band, from its position on the eastern end of the sub-band at the 1 km level, to its 3 km altitude position seen in Fig. 4b.

The divergence of the Doppler-derived wind field is shown in Fig. 4c. A band of convergence lay parallel to the large rainband seen in Fig. 4a. However, the convergence was concentrated in peaks associated with the three mesoscale features noted in the wind field. Maxima of convergence (at x = -24 km, y = 27 km and x = -25 km, y = 15 km) were just downwind of the two mesoscale wind speed maxima seen in Fig. 4b. A third and stronger maximum of convergence (only partially shown because of incomplete data coverage) is seen at x = -20 km, y = 8 km, near the center of the mesocyclone.

Also seen in Fig. 4c are two mesoscale areas of concentrated divergence. One is located just east of the convergence band, radially inside the large rainband (along x = -17 km, between y = 10 and 30 km). The other (centered at x = -17 km, y = -2 km) is associated with the region of strong diffluence seen just south of the mesocyclone in Fig. 4b.

The relative vorticity field (Fig. 4d) was also dominated by the mesoscale features seen in the wind field. A strong vorticity couplet (centered at x = -17 km, y = 37 km) was associated with the northern mesoscale wind maximum seen in Fig. 4b. This couplet lay just upwind of the northern convergence maximum seen in Fig. 4c. A corresponding couplet was not clearly associated with the weaker wind maximum to the south (at x = -21 km, y = 17 km in Fig. 4b). A major concentration of positive vorticity (centered at x = -20 km, y = 7 km) was associated with the mesocyclone. Thus, the positive vorticity in the portion of the developing hurricane that we have examined was concentrated in patches associated with discrete mesoscale features of the flow in the vicinity of the developing eyewall, especially near the mesocyclone.

6. CONCLUSIONS

Further analysis, carried out since our first report on the airborne Doppler radar observations obtained in the developing inner core of Hurricane Debby, has led to several new insights.

Fig. 4. Analysis of reflectivity and wind fields at the 3 km level derived from airborne Doppler radar data obtained in Hurricane Debby between 1950 and 2045 GMT 14 September 1982. Coordinates are east-west distance (x) and north-south distance (y) from the storm center. Each panel is a merger of analysis from Box 1 north of y = 10 and Box 2 south of y = 10. (a) Reflectivity contours for 30 and 40 dBZ. (b) Wind analysis. Plotting convention same as in Fig. 2. Winds exceeding 23 m/s are outlined by a heavy line. Values greater than 23 m/s are indicated by shading. (c) Contours of divergence for values of -3, 0, 3, 4, 5, 6, 7, and 8 x 10^{-3} s^{-1}. Zero line is heavy; positive contours are dashed; C and D indicate centers of convergence and divergence, respectively; regions where divergence calculations could not be made are left blank. (d) Contours of relative vorticity for values of -4, -2, 0, 2, 4, 6 and 8 x 10^{-3} s^{-1}. Zero line is heavy; negative contours are dashed; pluses and minuses indicate centers of positive and negative vorticity, respectively; regions where vorticity calculations could not be made are left blank.

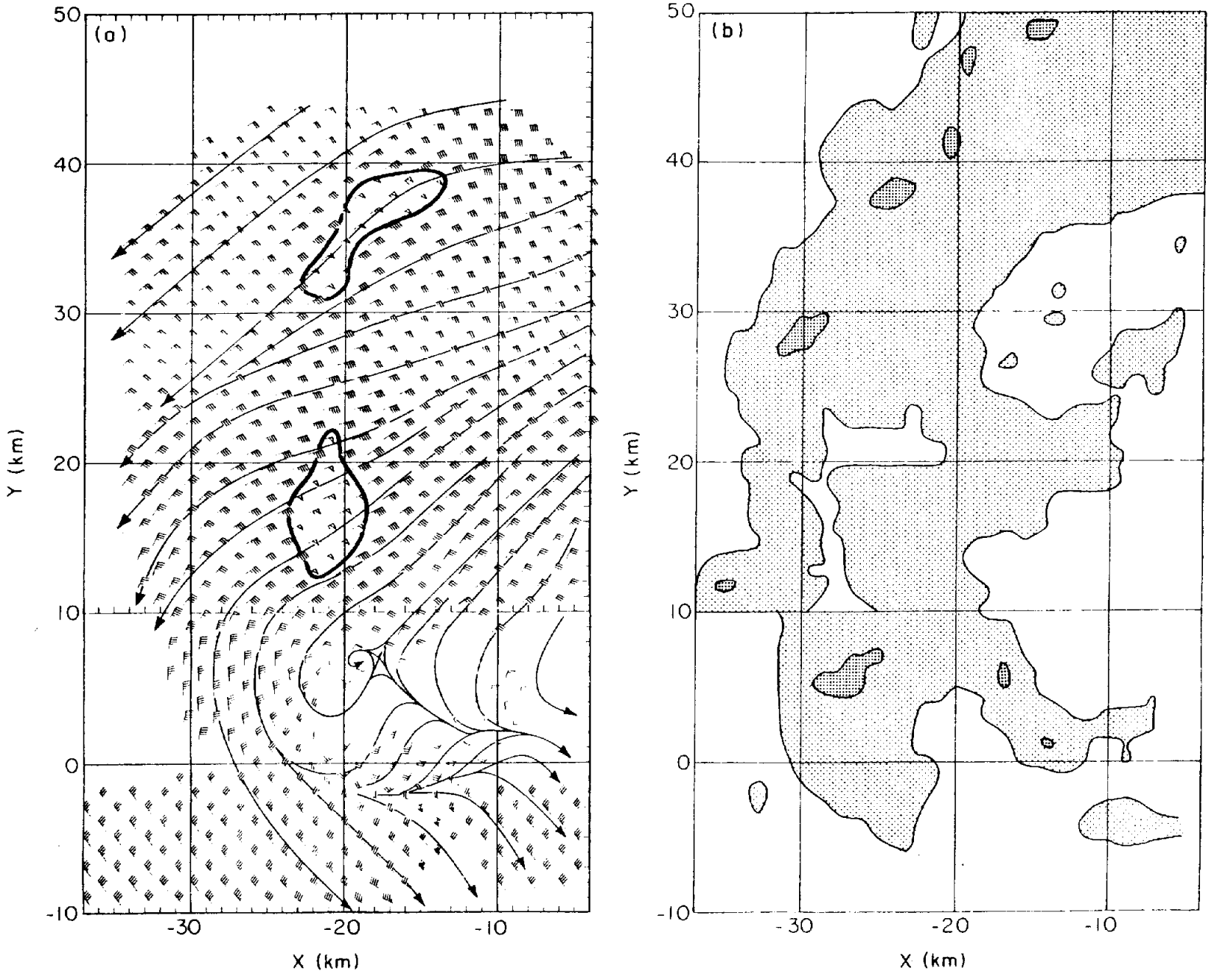
(a)
(b)
50
40
30
20
10
0
-10
-30
-20
-10
Y (km)
X (km)

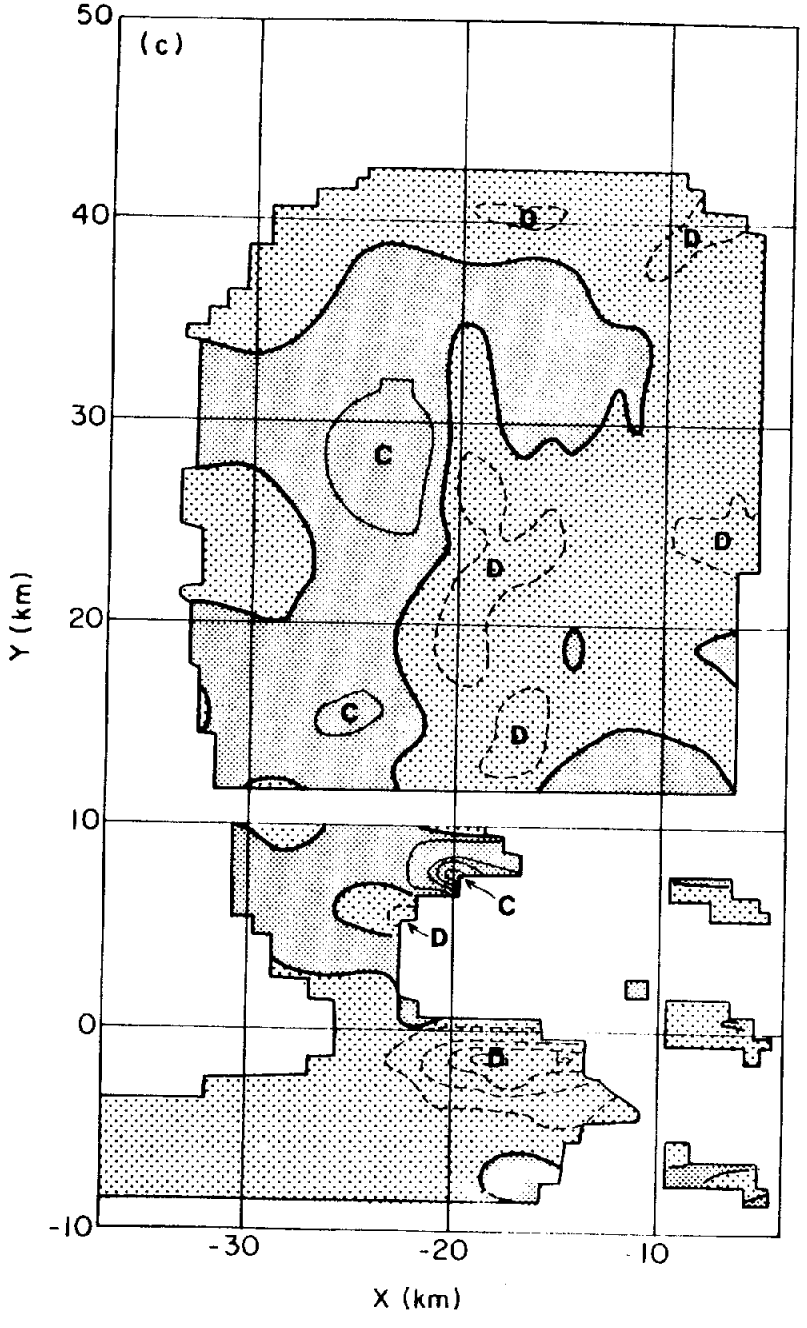
(c)
50
40
30
20
10
0
-10
-30
-20
-10
Y (km)
X (km)
C
D

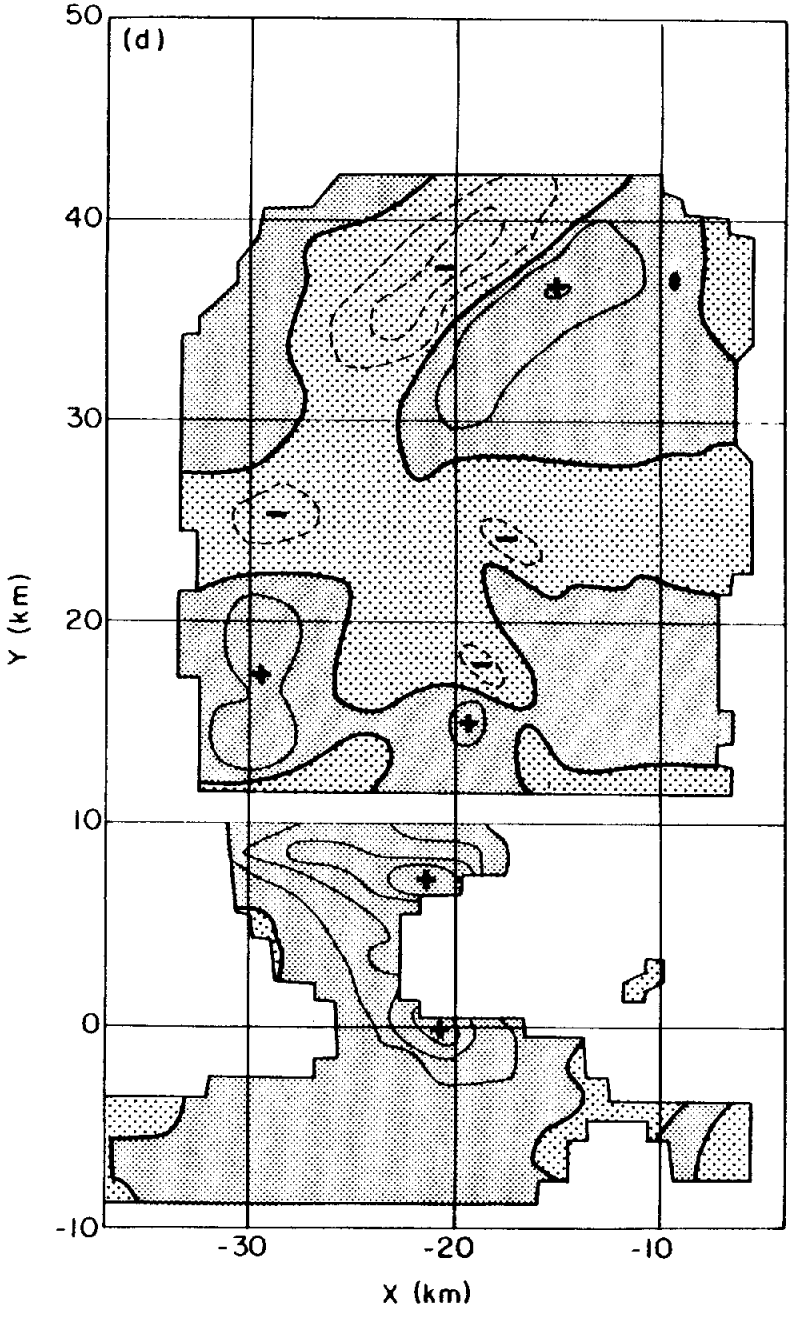
(d)
50
40
30
20
10
0
-10
-30
-20
-10
Y (km)
X (km)
+
-

Assessment of the quality of the data indicates that the Doppler-derived wind field in the vicinity of the developing eyewall is credible, while that in the stratiform regions west and southwest of the developing eyewall is suspect. Part of the problem may be that we have divided the analysis into overlapping regions, within each of which the wind is reconstructed from only the two nearest flight legs. It is likely that an improved analysis in the stratiform region could be obtained by adapting a method, such as the overdetermined dual Doppler technique described by Ray and Sangren (1983), in which the wind at any given point is determined as a best fit to data from all available viewing positions; in our case, from all three flight legs. For the present, however, we have restricted ourselves to drawing conclusions only from the credible analysis in the vicinity of the developing eyewall.

The inclusion of the Box 3 analysis allowed us to extend the analysis of the developing eyewall southward to include its full length. The flow associated with the developing eyewall was consistent with Jorgensen's (1984a,b) composite picture of mature eyewall structure deduced from aircraft flight-track data. However, the nearly instantaneous snapshot of the wind field provided by the airborne Doppler data shows that the wind structure in the developing eyewall region was concentrated in three distinct mesoscale disturbances.

Two of these disturbances were evident as mesoscale maxima in the 3 km level windspeed field. Each of these speed maxima was characterized by a convergence maximum immediately downwind. The better defined of the two wind maxima was also characterized by a vorticity couplet straddling the speed maximum.

The third mesoscale feature was a pronounced mesocyclone located along the southern part of the developing eyewall. This mesocyclone was associated with an intense sub-band in the precipitation pattern, and it contained most of the positive vorticity of the flow in the developing eyewall region. The positive vorticity in the mesocyclone was evidently being advected toward the center of the storm by the larger-scale, inwardly spiralling winds of the developing hurricane. This advection may have influenced the evolution of the hurricane.

Future studies should be directed toward determining the frequency of occurrence of wind maxima, mesocyclones and other mesoscale features embedded in the flows surrounding the inner cores of both developing and mature hurricanes. The dynamics of these features and their interactions with the storm-scale flow need to be understood. Airborne Doppler radar documentation of hurricane inner-core wind fields, together with parallel numerical modeling and theoretical efforts, should provide the means for tackling these problems over the next few years.

7. ACKNOWLEDGMENTS

The data used in this study were gathered with the aid of the NOAA Research Facilities Center flight crews and engineers, particularly Jim DuGranrut and Terry Schricker, who kept the airborne Doppler radar functioning during the 1982 Hurricane season. David Jorgensen helped design the Doppler analysis software. Thanks are extended to K. Moore for drafting the figures, C. Arthur for typing the text, and D. Churchill for final layout and copy. This research was supported partially by the National Science Foundation under Grant No. ATM 80-17327.

REFERENCES

Jorgensen, D. P., 1984a: Mesoscale and convective-scale characteristics of mature hurricanes. Part I: General observations by research aircraft. Submitted to J. Atmos. Sci.

Jorgensen, D. P., 1984b: Mesoscale and convective-scale characteristics of mature hurricanes. Part II. Inner core structure of Hurricane Allen (1980). Submitted to J. Atmos. Sci.

Marks, F. D., Jr., and R. A. Houze, Jr., 1983: Three-dimensional wind field in the developing inner core of Hurricane Debby. Preprints, 21st Conf. Radar Meteor., Amer. Meteor. Soc., Boston, 298-304.

Ray, P. S., and K. L. Sangren, 1983: Multiple-Doppler Radar Network Design. J. Climate Appl. Meteor., 22, 1444-1454.

Ray, P. S., R. J. Doviak, G. B. Walker, D. Sirmans, J. Carter, and B. Bumgarner, 1975: Dual-Doppler observation of a tornadic storm. J. Appl. Meteor., 14, 1521-1530.